NISTIR 6442

A Phase-Field Model with Convection: Numerical Simulations

D. M. Anderson
Department of Mathematical Sciences
George Mason University
Fairfax, VA 22030, USA

G. B. McFadden
U. S. DEPARTMENT OF COMMERCE
Technology Administration
National Institute of Standards
and Technology
Gaithersburg, MD 20899

A. A. Wheeler
Faculty of Mathematical Studies
University of Southampton
Highfield, Southampton, SO17 1BJ, UK

National Institute of Standards and Technology
Technology Administration
U.S. Department of Commerce

NISTIR 6442

A Phase-Field Model with Convection: Numerical Simulations

D. M. Anderson
Department of Mathematical Sciences
George Mason University
Fairfax, VA 22030, USA

G. B. McFadden
U. S. DEPARTMENT OF COMMERCE
Technology Administration
National Institute of Standards
and Technology
Gaithersburg, MD 20899

A. A. Wheeler
Faculty of Mathematical Studies
University of Southampton
Highfield, Southampton, SO17 1BJ, UK

December 15, 2000

U.S. DEPARTMENT OF COMMERCE
Norman Y. Mineta, Secretary

TECHNOLOGY ADMINISTRATION
Dr. Cheryl L. Shavers, Under Secretary
of Commerce for Technology

NATIONAL INSTITUTE OF STANDARDS
AND TECHNOLOGY
Raymond G. Kammer, Director

A PHASE-FIELD MODEL WITH CONVECTION: NUMERICAL SIMULATIONS

D.M. ANDERSON

Department of Mathematical Sciences, George Mason University, Fairfax, VA 22030, USA

G.B. MCFADDEN

Mathematical and Computational Sciences Division, National Institute of Standards and Technology, Gaithersburg, MD 20899-8910, USA

A.A. WHEELER

Faculty of Mathematical Studies, University of Southampton, Highfield, Southampton, SO17 1BJ, UK

In a previously-developed phase-field model of solidification that includes convection in the melt [1], the two phases are represented as viscous liquids, where the putative solid phase has a viscosity much larger than the liquid phase. In this paper we report numerical computations on a simplified form of this model which represents the growth of a two-dimensional dendrite in a thin gap between two parallel thermally insulting plates. In these computations flow in the liquid arises because of the differing densities of the solid and liquid phases.

1 Introduction

The notion of representing the boundary between two bulk thermodynamic phases as a diffuse interface dates back to the work of Poisson [2], Gibbs [3], Maxwell [4], Rayleigh [5], van der Waals [6] and Korteweg [7] in the 19th Century. The central assumption is that there is an interfacial *region* of small but nonzero thickness separating the two bulk phases. In such models, quantities such as surface tension, that in a sharp-interface description are regarded as localized on the interfacial *surface*, are instead recognized as being distributed through the interfacial region.

Diffuse interface models may be based on an extended thermodynamics that incorporates effects involving gradients of the thermodynamic variables ("nonclassical terms") to account for nonlocal effects. That a model incorporating a diffuse interface in this way is referred to as "nonclassical" is perhaps ironic in light of the above history, and speaks volumes for the success of the "classical" sharp-interface description of interfacial free boundary problems.

Despite the overall success of the classical approach, there are still special situations in which a diffuse-interface description of an interface between two bulk phases is a viable and even necessary approach. At least three types of situations may be identified. (i): The thickness of the interface becomes comparable to or larger than other mesoscopic length scales of interest in the problem. An example of such a situation is in the case of a fluid near its critical point, where the thickness of the interface diverges. Early diffuse interface models were developed to investigate this problem (see, e.g., van der Waals [6] and Rowlinson and Widom [8]). (ii): The length scales of interest in the problem under consideration are so small that they are comparable to the thickness of the interface. Contact line problems in fluid

mechanics (e.g. Davis [9]) are potentially in this category, as the diffuse nature of a fluid–fluid interface may become important at the small scales of interest near a contact line. In fact, recent calculations using diffuse-interface descriptions suggest that the force singularity associated with the classical free boundary description of a moving contact line (Dussan V. and Davis [10]) can be relieved when a nonzero interface thickness is taken into account (Jacqmin [11, 12], Seppecher [13]). (iii): A diffuse-interface formulation becomes a viable computational alternative to the classical free boundary problem when the morphology of the interface becomes very complicated or changes its topology. An important example is the solidification of dendrites, where sidearms branch from the main stem of the dendrite in a complicated dynamical process that involves both growth and subsequent coarsening behavior. Many successful computations of dendritic growth have now been performed [14–21].

Diffuse-interface theories have been developed and applied successfully in a wide range of other physical situations as well, such as superconductivity [22], liquid crystals [23], spinodal decomposition [24,25], ordering transitions in alloys [26–28], and a variety of hydrodynamic phenomena [29].

Our interest here concerns a phase-field model that accounts for both solidification and fluid motion. This work extends the phase-field model of the solidification of a pure material that was first proposed by Langer [30,31] and subsequently developed by a number of researchers [32–37]. Phase-field models provide an example of a diffuse-interface model in which an order parameter, ϕ, is postulated whose value indicates the phase of the system at a particular point in space and time (in this paper $\phi = 1$ and $\phi = 0$ denote the solid and liquid phases, respectively). Langer represented the free energy of a single-component system by a gradient energy functional of the form

$$\mathcal{F} = \int_V \left\{ \frac{1}{2}\epsilon^2 |\nabla\phi|^2 + f(\phi, T) \right\} dV, \tag{1}$$

where ϵ is the gradient energy coefficient and T is the temperature. The free energy density, $f(\phi, T)$, has a double-well structure with respect to ϕ in which the two local minima correspond to the solid and liquid phases. Langer proposed the following governing equations for the phase field and temperature:

$$M\frac{\partial\phi}{\partial t} = -\frac{\delta\mathcal{F}}{\delta\phi} = \left\{ \epsilon^2\nabla^2\phi - \frac{\partial f}{\partial\phi} \right\}, \tag{2}$$

$$c\frac{\partial T}{\partial t} = k\nabla^2 T + L\frac{\partial\phi}{\partial t}, \tag{3}$$

where $1/M$ is a positive constant termed the mobility, c is the heat capacity, k is the thermal conductivity and L is the latent heat per unit volume of the material. This phase-field formulation replaces the free-boundary problem associated with the sharp-interface model of an interface by a coupled pair of nonlinear reaction diffusion equations. The location of the interface is represented by the level set $\phi = 1/2$.

An early attempt to include fluid motion within a phase-field model of solidification is due to Caginalp and Jones [38,39]. They appended the inviscid momentum

equation and the continuity equation to the phase-field model, but did not address the issues of momentum balance in the solid and capillary contributions to the stress tensor. Diepers et al. [40, 41] have employed the methodology of two-phase fluid flow, where ϕ is interpreted as a solid fraction. Their model is used to study coarsening in a binary solid/liquid mixture with and without fluid flow. Tönhardt and Amberg have also performed two-dimensional numerical studies using adaptive finite elements. They study the effect of a shear flow on dendritic growth morphology and show preferential side-branching on the upstream side of the dendrite [42, 43].

In this paper we briefly describe a recently-developed phase-field model [1] which allows for convection in the liquid phase. This model has three notable aspects: first, we represent both the solid and liquid phases as Newtonian fluids in which the viscosity of the putative solid phase is specified to be much larger than that of the liquid phase. Second, the interface is ascribed an anisotropic surface energy. Third, the phase transition is considered to be first order. These features are non-standard for a model which treats the two phases as Newtonian fluids, but is in keeping with our intention to model a solid-liquid system. We note that in many solidification applications, a fluid model is used for the thermodynamic description of the solid phase, in that the elastic properties of the solid are ignored. In order to obtain the desired viscosity variation between the phases, the viscosity is assumed to depend on the phase field, ϕ. The anisotropic surface energy is achieved by employing the generalized ξ-vector formalism [44]. Unlike previous diffuse interface models, which incorporate fluid motion coupled to a conserved order parameter description [29], we adopt a nonconserved order parameter, ϕ, in line with our aim of directly extending conventional phase-field models of solidification to account for convection. This has the advantage that we may treat quasi-incompressible systems [45], in which the density field is taken to be a prescribed function of ϕ.

We sketch how the model may derived in the setting of irreversible thermodynamics. The quasi-incompressibility assumption restricts the form of the thermodynamic potentials that may be employed [45]. The model comprises the compressible Navier-Stokes equations with a modified stress tensor that includes additional terms related to gradients of ϕ, an energy equation, and a phase-field equation involving a material time derivative of ϕ. We go on to describe computations based on a simplified form of this phase-field model. In particular, we study a configuration in which a dendrite grows into an undercooled liquid between two thermally insulating plates. This allows us to avoid directly solving the generalized compressible Navier-Stokes equations by adopting a Hele-Shaw approximation. The densities of the solid and liquid phases are allowed to differ, and we study numerically the effect of the density-induced flow on the growth of the dendrite.

2 The Model

We consider a non-isothermal system consisting of a pure material that may exist in two distinct phases. We follow the standard phase-field methodology and introduce a phase-field variable, $\phi(\vec{x}, t)$, whose value indicates the thermodynamic phase of the system as a function of position, $\vec{x}$, and time, t. A solid-liquid interface is represented by a thin layer in which the phase field varies rapidly between zero

(liquid) and unity (solid). The governing equations are derived by following the formalism of irreversible thermodynamics [37, 46–48] as described below.

2.1 Governing Equations

We assume that the total entropy, $\mathcal{S}$, in a material volume, $\Omega(t)$, of the system is given by

$$\mathcal{S} = \int_{\Omega(t)} \left[\rho s - \frac{1}{2}\epsilon_S^2 \Gamma^2(\nabla\phi) \right] dV, \tag{4}$$

where ρ is the density and s is the entropy per unit mass. The first term in the integrand, ρs, is the classical entropy density per unit volume and the second is a nonclassical term associated with spatial gradients of the phase field. Here the gradient entropy coefficient ϵ_S is assumed to be a constant for simplicity, and Γ is a homogeneous function of degree unity. The function Γ allows for a general anisotropic surface energy of the solid-liquid interface and allows the Cahn-Hoffman ξ-vector formalism for sharp interfaces [49, 50] to be generalized and extended to diffuse interface models [44, 51]. An isotropic surface energy results from the choice $\Gamma(\nabla\phi) = |\nabla\phi|$.

The total mass, $\mathcal{M}$, linear momentum, $\vec{\mathcal{P}}$, and internal energy, $\mathcal{E}$, associated with the material volume are assumed to have the form

$$\mathcal{M} = \int_{\Omega(t)} \rho \, dV, \tag{5}$$

$$\vec{\mathcal{P}} = \int_{\Omega(t)} \rho\vec{u} \, dV, \tag{6}$$

$$\mathcal{E} = \int_{\Omega(t)} \left[\rho e + \frac{1}{2}\rho|\vec{u}|^2 + \frac{1}{2}\epsilon_E^2 \Gamma^2(\nabla\phi) \right] dV, \tag{7}$$

respectively. Here $\vec{u}$ is the velocity, e is the internal energy density per unit mass and ϵ_E is the gradient energy coefficient, which is assumed to be constant. The thermodynamic relations

$$de = T\,ds + \frac{p}{\rho^2}\,d\rho + \frac{\partial e}{\partial \phi}\,d\phi, \tag{8}$$

$$e = Ts - p/\rho + \mu, \tag{9}$$

are assumed to apply locally, where p is the thermodynamic pressure and μ is the chemical potential (or Gibbs free energy per unit mass).

The physical balance laws for mass, linear momentum, and internal energy are given by

$$\frac{d\mathcal{M}}{dt} = 0, \tag{10}$$

$$\frac{d\vec{\mathcal{P}}}{dt} = \int_{\delta\Omega(t)} \hat{n} \cdot m \, dA, \tag{11}$$

$$\frac{d\mathcal{E}}{dt} + \int_{\delta\Omega(t)} \vec{q}_E \cdot \hat{n} \, dA = \int_{\delta\Omega(t)} \hat{n} \cdot m \cdot \vec{u} \, dA, \tag{12}$$

respectively, where $\hat{n}$ is the outward unit normal to $\delta\Omega(t)$, m is the stress tensor, and $\vec{q}_E$ is the internal energy flux. The momentum balance (11) requires that the rate of change of the total momentum of the material volume results from forces acting on its boundary $\delta\Omega(t)$ (for simplicity we neglect body forces such as gravity; their inclusion is straightforward). The energy balance (12) equates the rate of change of the total internal energy of $\Omega(t)$ plus the energy flux through its boundary to the rate of work of the forces at its boundary.

In addition, the entropy balance takes the form

$$\frac{dS}{dt} + \int_{\delta\Omega(t)} \vec{q}_S \cdot \hat{n}\, dA = \int_{\Omega(t)} \dot{s}_{prod}\, dV, \tag{13}$$

where $\vec{q}_S$ is the entropy flux and $\dot{s}_{prod}$ is the local rate of entropy production. The second law of thermodynamics is then expressed by the requirement that $\dot{s}_{prod}$ is non-negative.

To proceed we recast the conservation laws (10)–(13) as differential equations. These are used to express the local entropy production in terms of the fluxes m, $\vec{q}_E$, and $\vec{q}_S$, as well as $D\phi/Dt$. We then identify forms for these quantities which ensure that the local entropy production is non-negative. The fluxes that result from this procedure involve both classical contributions and non-classical contributions that depend on $\nabla\phi$. In addition, we obtain an evolution equation for the phase field. The details of this procedure are given in Ref. [1] and result in the following governing equations:

$$\frac{D\rho}{Dt} = -\rho\nabla\cdot\vec{u}, \tag{14}$$

$$\rho\frac{D\vec{u}}{Dt} = \nabla\cdot m, \tag{15}$$

$$M\frac{D\phi}{Dt} = \epsilon_F^2(T)\nabla\cdot[\Gamma(\nabla\phi)\vec{\xi}] - \rho\frac{\partial g}{\partial\phi}, \tag{16}$$

$$\rho\frac{De}{Dt} = \nabla\cdot[k\nabla T] + \epsilon_E^2\nabla\cdot\left[\Gamma(\nabla\phi)\vec{\xi}\right]\frac{D\phi}{Dt} + m_S : \nabla\vec{u}, \tag{17}$$

where $1/M$ is a mobility, m is the stress tensor [see equation (23)], m_S is a modified stress tensor [see equation (24)], ϵ_F is the Helmholtz gradient energy coefficient given by $\epsilon_F^2(T) = \epsilon_E^2 + T\epsilon_S^2$, $g(T,p,\phi) = e - Ts + p/\rho$ is the Gibbs free energy per unit mass, and $\vec{\xi}$ is the generalized ξ-vector [44] whose components are defined by $\xi_j = \partial\Gamma(\vec{p})/\partial p_j$, where we have written $\vec{p} = \nabla\phi$. The density of the two bulk phases may be different, and we will assume that ρ depends on ϕ alone,

$$\rho(\phi) = \rho_S r(\phi) + \rho_L[1 - r(\phi)], \tag{18}$$

where $r(\phi)$ is a monotonic increasing function with $r(0) = 0$ and $r(1) = 1$; suitable choices include $r(\phi) = \phi$ or $r(\phi) = \phi^2(3-2\phi)$. This assumption, in which the density does not depend on temperature or pressure, is known as quasi-incompressibility, as it still allows a nonzero divergence of the velocity vector. This assumption places a constraint on the form of the underlying thermodynamic potentials [45] which requires the underlying Gibbs free energy (per unit mass) to have the form

$$g(T,p,\phi) = g_0(T,\phi) + \frac{(p - p_0)}{\rho(\phi)}, \tag{19}$$

where p_0 is a reference pressure. Here we assume that the function $g_0(T,\phi)$ has the form

$$g_0(T,\phi) = \left[e_0 - cT_M - r(\phi)L - \frac{1}{4a_S}H(\phi)\right]\left(1 - \frac{T}{T_M}\right) - cT\ln\left(\frac{T}{T_M}\right) + \frac{1}{4a}H(\phi), \tag{20}$$

in which case the corresponding expressions for the internal energy and entropy densities are

$$e = e_0 + c(T - T_M) - r(\phi)L + \frac{1}{4a_E}H(\phi) - \frac{p_0}{\rho(\phi)}, \tag{21}$$

$$s = \frac{1}{T_M}\left[e_0 - r(\phi)L - \frac{1}{4a_S}H(\phi)\right] + c\ln\left(\frac{T}{T_M}\right), \tag{22}$$

where $1/a_E = 1/a - 1/a_S$. Here $1/a$ is the height of the double well of the Gibbs free energy density at $T = T_M$, and $1/a_E$ and $1/a_S$ are the heights of the double wells in the internal energy and entropy densities, respectively. The double well potential $H(\phi)$ is a prescribed function of ϕ (see [56]). The quantity e_0 is a constant reference energy and both the heat capacity per unit mass c and the latent heat per unit mass L are assumed to be constant. T_M is the melting point at the reference pressure p_0.

The tensors m and m_S are given by

$$m = \left[-p + \frac{\epsilon_F^2(T)}{2}\Gamma^2(\nabla\phi)\right] I - \epsilon_F^2(T)\Gamma(\nabla\phi)\vec{\xi}\otimes\nabla\phi + \tau, \tag{23}$$

$$m_S = \left[-p + \frac{T\epsilon_S^2}{2}\Gamma^2(\nabla\phi)\right] I - T\epsilon_S^2\Gamma(\nabla\phi)\vec{\xi}\otimes\nabla\phi + \tau, \tag{24}$$

where τ is the viscous stress tensor,

$$\tau = \mu\left[\nabla\vec{u} + (\nabla\vec{u})^T - \frac{2}{3}(\nabla\cdot\vec{u})\ I\right], \tag{25}$$

and μ is the viscosity, which is a function of ϕ,

$$\mu(\phi) = \mu_S r(\phi) + \mu_L[1 - r(\phi)]. \tag{26}$$

By examining the isothermal one-dimensional solution of the governing equations at the melting temperature T_M with $\rho_S = \rho_L$, it may be shown that the surface tension γ, interface thickness l, and interface attachment coefficient μ_0 are related to the phase-field parameters by

$$\gamma(\vec{n}) = \frac{\epsilon_F(T_M)}{6}\Gamma(\vec{n})\sqrt{\frac{\rho_L}{2a}}, \quad l(\vec{n}) = \epsilon_F(T_M)\Gamma(\vec{n})\sqrt{\frac{2a}{\rho_L}}, \quad \mu_0(\vec{n}) = \frac{6\rho_L L l\Gamma(\vec{n})}{T_M M}. \tag{27}$$

We will henceforth confine our attention to case of isotropic surface energies and set $\Gamma(\nabla\phi) = |\nabla\phi|$; in this case we note that $\Gamma(\vec{n}) = 1$. It is also convenient to define an associated capillary length by $l_c = T_M\gamma/(\rho_L[L^2/c])$.

2.2 Dimensionless Governing Equations

We non-dimensionalize the governing equations by introducing the following dimensionless variables, which we denote with a prime:

$$\vec{x} = l_0\vec{x}', \quad t = \frac{l_0^2}{\kappa_L}t', \quad \vec{u} = \frac{\kappa_L}{l_0}\vec{u}', \quad \boldsymbol{m} = \frac{\rho_L\kappa_L^2}{l_0^2}\boldsymbol{m}', \quad p = p_0 + \frac{\rho_L\kappa_L^2}{l_0^2}p', \tag{28}$$

$$T = T_M + \frac{L}{c}\theta', \quad \rho = \rho_L\rho', \quad \mu = \mu_L\mu', \quad k = k_Lk'. \tag{29}$$

Here the reference length scale l_0 is a typical length scale associated with the interface shape, such as a dendrite tip radius, the reference time scale is l_0^2/κ_L, and the reference velocity scale is $U = \kappa_L/l_0$, where κ_L is the thermal diffusivity in the bulk liquid phase. The dimensionless governing equations are

$$\frac{\partial\rho}{\partial t} + \nabla\cdot(\rho\vec{u}) = 0, \tag{30}$$

$$\rho\frac{D\vec{u}}{Dt} = \nabla\cdot\boldsymbol{m}, \tag{31}$$

$$\epsilon^2\widetilde{M}\frac{D\phi}{Dt} = \epsilon^2(1+\alpha\theta)\nabla^2\phi - \rho\left[\frac{1}{2}(1+\beta\theta)H'(\phi) + \lambda\theta r'(\phi) + \frac{\epsilon}{\tilde{\gamma}}p\frac{\partial}{\partial\phi}\left(\frac{1}{\rho}\right)\right], \tag{32}$$

$$\rho\frac{De}{Dt} = \nabla\cdot[Q(\phi)\nabla\theta] + \epsilon^2\nu\frac{D\phi}{Dt}\nabla^2\phi + \mathcal{H}, \tag{33}$$

where, for simplicity, we have omitted the primes on the dimensionless variables. The dimensionless internal energy density is given by

$$e = \theta - r(\phi) + \frac{\delta}{2}H(\phi) - \frac{\epsilon Sp^\star}{\lambda\tilde{\gamma}}\frac{1}{\rho}, \tag{34}$$

and the dimensionless stress tensors are

$$\boldsymbol{m} = \boldsymbol{\sigma}^p + (1+\alpha\theta)\boldsymbol{\sigma}^\phi + Pr\boldsymbol{\tau}, \tag{35}$$

$$\boldsymbol{m}_S = \boldsymbol{\sigma}^p + \alpha(\theta + S^{-1})\boldsymbol{\sigma}^\phi + Pr\boldsymbol{\tau}, \tag{36}$$

where $Pr = \nu_L/\kappa_L$ is the Prandtl number of the liquid phase, ν_L is the kinematic viscosity of the liquid phase and

$$\boldsymbol{\sigma}^p = -(p+p^\star)\boldsymbol{I}, \tag{37}$$

$$\boldsymbol{\sigma}^\phi = \tilde{\gamma}\epsilon\left[\frac{1}{2}|\nabla\phi|^2\boldsymbol{I} - \nabla\phi\otimes\nabla\phi\right], \tag{38}$$

$$\boldsymbol{\tau} = \mu(\phi)\left[\nabla\vec{u} + (\nabla\vec{u})^T - \frac{2}{3}(\nabla\cdot\vec{u})\ \boldsymbol{I}\right]. \tag{39}$$

The source term in the energy equation is

$$\mathcal{H} = \frac{\epsilon S}{\lambda\tilde{\gamma}}\boldsymbol{m}_S : \nabla\vec{u} = \frac{\epsilon S}{\lambda\tilde{\gamma}}\left[-(p+p^\star)\boldsymbol{I} + \alpha\left(\theta + S^{-1}\right)\boldsymbol{\sigma}^\phi + Pr\boldsymbol{\tau}\right] : \nabla\vec{u}, \tag{40}$$

and the dimensionless parameters are given by

$$\alpha = \frac{L\epsilon_S^2}{c\epsilon_F^2(T_M)}, \quad \beta = \frac{aL}{a_S c T_M}, \quad \delta = \frac{1}{2a_E L}, \quad \nu = \frac{\epsilon_E^2}{l^2 L \rho_L} = \frac{\epsilon_E^2}{2aL\epsilon_F^2(T_M)}, \tag{41}$$

$$\epsilon = \frac{l}{l_0}, \quad \lambda = \frac{l}{6l_c}, \quad p^\star = \frac{p_0 l_0^2}{\rho_L \kappa_L^2}, \quad S = \frac{L}{cT_M} \tag{42}$$

$$\widetilde{\gamma} = \frac{6l_0 l_c L^2}{\kappa_L^2 c T_M} = \frac{6l_0\gamma}{\rho_L \kappa_L^2}, \quad \widetilde{M} = \frac{\kappa_L M T_M c}{6\rho_L l l_c L^2} = \frac{[\kappa_L/l_c]}{[L/c]\mu_0}, \tag{43}$$

and

$$Q(\phi) = 1 + \left(\frac{k_S}{k_L} - 1\right) r(\phi), \quad \mu(\phi) = 1 + \left(\frac{\mu_S}{\mu_L} - 1\right) r(\phi), \quad \rho(\phi) = 1 + \left(\frac{\rho_S}{\rho_L} - 1\right) r(\phi). \tag{44}$$

We note that the parameter $\widetilde{\gamma}$ is related to the capillary (or crispation) number Ca by $\widetilde{\gamma} = 6Pr/Ca$, where $Ca = \mu_L \kappa_L/(l_0\gamma)$.

In the absence of flow these equations reduce to the generalized phase-field equations recently studied in Refs. [52] and [53]. The leading-order free boundary problem that emerges from a sharp-interface limit of these equations depends on the distinguished limit that is taken [54, 55, 52]. The limit in which $\lambda = \mathcal{O}(1)$ as $\epsilon \to 0$ corresponds to the so-called 'thin interface' limit studied by Karma and Rappell [55]. In this analysis when the thermal conductivities of the solid and liquid phases are unequal the leading-order temperature is discontinuous across the interface and the leading-order modified Gibbs-Thomson equation contains terms dependent on the interfacial temperature gradients. However, if $\lambda = \mathcal{O}(\epsilon)$ as $\epsilon \to 0$, the so-called 'classical' limit, the temperature is continuous across the interface at leading order and a nonlinear form of the modified Gibbs-Thomson equation is obtained at leading order. However, if we formally set the coefficients α, β, δ, and ν to zero, thereby omitting the nonstandard terms in the generalized phase-field equations, then the classical sharp interface analysis recovers, at leading order, a standard free boundary problem in which the interfacial temperature is continuous and the conventional modified Gibbs-Thomson equation is obtained.

Here we study a simplified form of our model by setting the constants α, β, δ, and ν to zero, and we neglect the source term $\mathcal{H}$ in the energy equation. The dimensionless governing equations of the simplified model are

$$\frac{\partial \rho}{\partial t} + \nabla \cdot (\rho \vec{u}) = 0, \tag{45}$$

$$\rho \frac{D\vec{u}}{Dt} = \nabla \cdot m, \tag{46}$$

$$\epsilon^2 \widetilde{M} \frac{D\phi}{Dt} = \epsilon^2 \nabla^2 \phi - \rho \left[\frac{1}{2} H'(\phi) + \lambda\theta r'(\phi) + \frac{\epsilon}{\widetilde{\gamma}} p \frac{\partial}{\partial \phi}\left(\frac{1}{\rho}\right)\right], \tag{47}$$

$$\rho \frac{De}{Dt} = \nabla \cdot [Q(\phi)\nabla\theta], \tag{48}$$

where the dimensionless stress tensor is

$$m = \sigma^p + \sigma^\phi + Pr\tau. \tag{49}$$

We have recently examined the full system of governing equations, including flow, in the sharp-interface limit [56]. Our investigations reveal that, in the classical sharp-interface limit, the boundary conditions at a sharp interface in equilibrium comprise the normal stress balance including surface tension and the Clausius-Clayperon equation all under isothermal conditions. In the nonequilibrium case we find hydrodynamic conditions on the normal and tangential velocities representing the conservation of mass and the no-slip condition. Jumps conditions on the normal and tangential stresses are also obtained. The temperature is found to be continuous across the interface while the jump in heat flux across the interface is modified by nonequilibrium effects. The temperature of the interface found to obey a nonequilibrium version of the Clausius–Clapeyron relation.

3 Model Computations

We now describe computations, based upon the phase-field model given by equations (45), (46), (47), (48) and (49), that represent the density change flow associated with the growth of a dendrite from an undercooled melt. To proceed we make a number of additional approximations in order to develop a simplified phase-field model that captures the qualitative features of this situation. First, we consider the dendrite to be two-dimensional and growing in a uniform thin gap of width d between two thermally insulated flat plates. This allows us to ignore the effects of inertia and to model the flow using a Hele-Shaw approximation. The momentum equation may then be written as

$$\nabla\left(-\frac{1}{\tilde{\gamma}}p + \frac{\epsilon}{2}|\nabla\phi|^2\right) - \epsilon\nabla\cdot[\nabla\phi\otimes\nabla\phi] + \frac{Ca}{6}\nabla\cdot[\mu(\phi)\tau] = 0. \tag{50}$$

In the absence of flow it is known that it is essential to include surface energy anisotropy in order to compute dendritic structures using a phase-field model [14]. We will accordingly retain anisotropic surface energy terms in the phase-field equation alone. Specifically, an isotropic surface energy term is used in the momentum equation (50) while the phase-field equation, given by (47), is modified to allow for anisotropic surface energy by using the Cahn-Hoffman ξ-vector formalism

$$\epsilon^2\widetilde{M}\frac{D\phi}{Dt} = \epsilon^2\nabla\cdot[\Gamma(\nabla)\vec{\xi}] - \rho\left[\frac{1}{2}H'(\phi) + \lambda\theta r'(\phi)\right], \tag{51}$$

so that the direct effect of anisotropy is upon the interfacial surface energy rather than the flow. We note we have also omitted the pressure dependence in the free energy term in the phase-field equation. This is a reasonable approximation for density-driven flows, as evidenced by the insignificant variations of the melting temperature due to pressure fluctuations in the Clausius-Clayperon relation under these conditions.

In order to simplify the system further we make the approximation $\nabla\cdot(\nabla\phi\otimes\nabla\phi) \approx \nabla(|\nabla\phi|^2)$. This approximation is exact in one space dimension, but not

higher dimensions. We justify it by observing that the phase-field variable only changes in the thin interfacial regions where it depends primarily on the perpendicular distance through the layer and hence is approximately one dimensional. Using this approximation the momentum equation (50) becomes

$$-\nabla \bar{p} + \frac{Ca}{6} \nabla \cdot [\mu(\phi)\tau] = 0, \tag{52}$$

where

$$\bar{p} = \frac{1}{\tilde{\gamma}} p + \frac{\epsilon}{2} |\nabla \phi|^2. \tag{53}$$

We now integrate these equations across the narrow gap of width $d \ll 1$ [58] to obtain

$$\vec{u} = \frac{-3d^2}{Ca\ \mu(\phi)} \left(\frac{z}{d}\right) \left(\frac{d-z}{d}\right) \nabla \bar{p}, \tag{54}$$

where here and below the operator ∇ acts in the plane parallel to the thin gap. We now apply the continuity equation (45) to find that $\bar{p}$ satisfies

$$\nabla^2 \bar{p} = \frac{2Ca}{d^2} \mu(\phi) \frac{\rho'(\phi)}{\rho(\phi)} \frac{\partial \phi}{\partial t} + \left[\frac{\mu'(\phi)}{\mu(\phi)} - \frac{\rho'(\phi)}{\rho(\phi)}\right] \nabla \phi \cdot \nabla \bar{p}. \tag{55}$$

In our numerical computations we solved the energy equation (48), phase-field equation (51) and pressure equation (55) using VLUGR [57]. This freely distributed package is designed to solve systems of parabolic partial differential equations in which the solution exhibits regions in space with large gradients. It employs a finite-difference discretization allied to local grid refinement and a variable time step integration of the underlying discretized equations.

Computations were conducted on the rectangular domain $[0, X] \times [0, Y]$. Neumann boundary conditions were employed on ϕ and θ on all four sides. However, for the pressure, Neumann boundary conditions were only invoked on the sides $x = 0$ and $y = 0$, with Dirichlet boundary conditions on the other two sides. The initial condition represented a small circular solid region centered on the origin in a uniformly undercooled melt with dimensionless temperature $\mathcal{T} = c(T_M - T_0)/L$, where T_0 is the initial dimensional temperature.

The governing equations were solved with $\rho(\phi)$ given by Eqn. (44), $r'(\phi) = 30\phi^2(1-\phi)^2$ and $H(\phi) = \phi^2(1-\phi)^2$. The surface energy had a four-fold anisotropy with $\Gamma(\vec{n}) = 1 + 0.005\cos(4\Theta)$, where $\vec{n} = \nabla\phi/|\nabla\phi|$ is a unit vector in the (x, y) plane and Θ is the angle between $\vec{n}$ and the x-axis. The values of the dimensionless parameters used in the computations are given by $Ca = 30$, $\mu_S/\mu_L = 1$, $k_S/k_L = 1$, $\lambda = 7.5$, and $\widetilde{M} = 10$.

In Figure 1 we display the results of a typical computation in which $\rho_S/\rho_L = 0.9$, $X = 1$, and $Y = 3$. This figure shows the pressure field, the velocity field and the phase field at time $t = 0.3$. The solid curves are isobars, the arrows represent the local velocity, and the shading indicates the phase field. The x and y axes represent planes of symmetry in the calculation, although since $X \neq Y$ the resulting shape has two-fold but not four-fold symmetry due to the presence of the sidewalls. The dendrite growing in the x direction has a blunter tip than the dendrite growing in

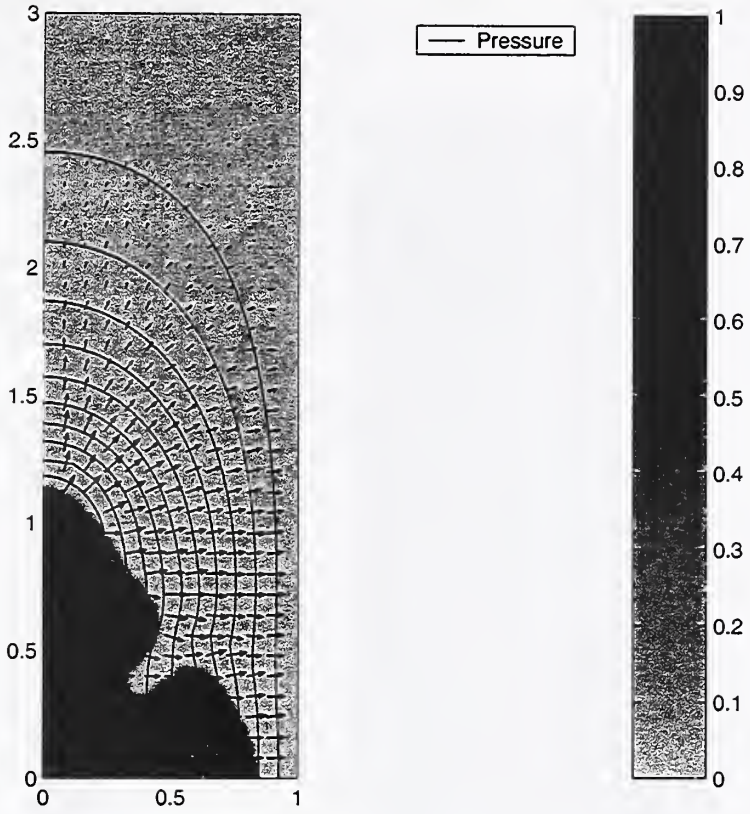

Figure 1. The phase-field, pressure field and velocity field for a computation at $t = 0.3$ with $\rho_S/\rho_L = 0.9$ on a 1×3 domain with four-fold anisotropy. The colors indicate the liquid ($\phi = 0$) and solid ($\phi = 1$) region, the solid curves are the isobars, and the small arrows represent the velocity field.

the y direction due to its closer proximity to the sidewall, which has a significant effect on the growth dynamics at this stage.

Since the density of the solid is less than that of the liquid, a given amount of material will expand upon solidification, which drives a flow away from the interface into the melt. For a sharp-interface model, the conservation of mass boundary condition takes the form

$$u_n = -v_n \left(\frac{\rho_S}{\rho_L} - 1 \right), \tag{56}$$

where $u_n = \vec{n} \cdot \vec{u}$ is the normal component of the fluid velocity at the interface, and v_n is the normal velocity of the interface. Thus for solidification with $v_n > 0$, the flow is away from the interface ($u_n > 0$) for $\rho_S < \rho_L$, and is toward the interface ($u_n < 0$) for $\rho_S > \rho_L$. The computation shows that the flow is greatest in the vicinity of the tip of the dendrite. For this calculation with equal viscosities in the solid and liquid phases, there is also a significant flow in the solid region. This

artifact is reduced for computations with $\mu_S/\mu_L \gg 1$; here we are illustrating an extreme example of this effect.

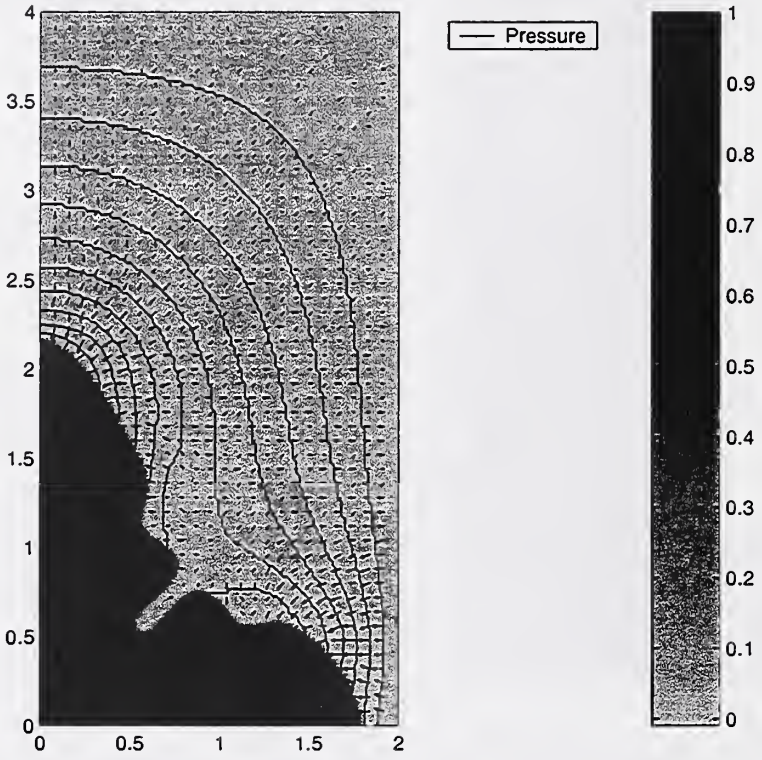

Figure 2. The phase-field, pressure field and velocity field at $t = 0.75$ for a computation with $\rho_S/\rho_L = 1.1$ on a 2×4 domain with four-fold anisotropy. The colors indicate the liquid ($\phi = 0$) and solid ($\phi = 1$) regions, the solid curves are the isobars, and the small arrows represent the velocity field.

Figure 2 shows a similar situation but with the density in the solid greater than that of the liquid, $\rho_S/\rho_L = 1.1$, with $X = 2$ and $Y = 4$ at a time $t = 0.75$. In this case the advection is toward the interface, as expected. Between the two dendrite tips is a narrow liquid intrusion where little solidification is taking place; the flow velocities that are induced by the density change upon solidification are correspondingly small in this region.

4 Conclusions

In this paper we have shown that computations based on a simplified form of a recent phase-field model that includes convection [1] exhibits numerical solutions which show the expected physical behavior. In particular, we considered the growth of a dendrite in a thin gap between two thermally insulated plates and allowed the

density of the solid and liquid phases to be different. We found that the flow was directed towards or away from the dendrite depending on whether the density of the solid phase was greater or less than that of the liquid phase, respectively.

Our model for solidification with convection is derived using the formalism of irreversible thermodynamics, and allows the systematic incorporation of a consistent thermodynamic description of the two-phase system. It allows a unified treatment of both equilibrium and non-equilibrium effects in a single set of governing equations. Sharp-interface limits of the diffuse-interface description then lead to boundary conditions of the solid-liquid interface which recover the usual conditions at equilibrium, and provide thermodynamically-consistent generalizations of these conditions under non-equilibrium conditions [56]. The detailed nature of the non-equilibrium conditions at the interface can be sensitive to the specific forms that are assumed to describe the variation of the thermophysical parameters through the interfacial region; for example, the non-equilibrium solute trapping behavior of a diffuse-interface model of a binary alloy depends quantitatively on the exact form that is assumed for the variation of solute diffusivity, $D(\phi)$, near the interface [59].

In this model the solid is treated as a liquid with high viscosity. This allows residual convection to occur in the solid, with a magnitude that is determined by the viscosity ratio. The consideration of extreme viscosity ratios tends to eliminate velocity gradients in the solid, but allows states of uniform convection that correspond to rigid body motion. This is an attractive feature for dealing with such issues as fragmentation and subsequent motion of sidearms through the melt. Such transported fragments can serve as sites for the growth of independent grains when the fragments are incorporated into the growing phase, which is a problem of considerable technological importance. It is thus beneficial to have a model which allows for both topological changes in the interface as well as possible rigid-body motion of the solid phase.

5 Acknowledgments

The authors dedicate this work to Professor S.H. Davis in honor of his sixtieth birthday. We would like to express our most sincere gratitude to Steve for the wide range of contributions he has made to our careers as teacher, colleague, and friend. The authors are also grateful for helpful discussions with W.J. Boettinger, T.J. Burns, S.R. Coriell, and R.F. Sekerka during the preparation of this manuscript. This research was conducted with the support of the Microgravity Research Division of NASA.

References

1. D. M. Anderson, G. B. McFadden and A. A. Wheeler, Physica D **135**, 175 (2000).
2. S. D. Poisson, (1831) Paris: Bachelier.
3. J. W. Gibbs, *Scientific Papers of J. Willard Gibbs*, ed. H. A. Bumstead and R.G. Van Name, (Longmans, Green, and Co., London, 1928) pp. 55-371.
4. J. C. Maxwell, in *Scientific Papers of James Clerk Maxwell*, Vol 2, (Dover,

New York, 1952) pp. 541–591.
5. Lord Rayleigh, Phil. Mag. **33**, 209 (1892).
6. J. D. van der Waals, Verhandel. Konink. Akad. Weten. Amsterdam (Sect. 1), vol. 1, No. 8 (1893); Transl. from Dutch: JS Rowlinson, J. Stat. Phys. **20**, 197 (1979).
7. D. J. Korteweg, Arch. Néerl. Sci. Exactes Nat. Ser. II **6**, 1 (1901).
8. J. S. Rowlinson and B. Widom, Molecular Theory of Capillarity (Clarendon, Oxford, 1989).
9. S. H. Davis, J. Appl. Mech. **50**, 977 (1983).
10. E. B. Dussan V and S.H. Davis, J. Fluid Mech. **65**, 71 (1974).
11. D. Jacqmin, J. Comput. Physics **155**, 96 (1999).
12. D. Jacqmin, J. Fluid Mech. **402**, 57 (2000)
13. P. Seppecher, Int. J. Engng. Sci. **34**, 977 (1996).
14. R. Kobayashi, Physica D **63**, 410 (1993).
15. A. A. Wheeler, B. T. Murray, R. J. Schaefer, Physica D **66**, 243 (1993).
16. J. A. Warren and W. J. Boettinger, Acta. metall. mater. **43**, 689 (1995) 689.
17. S.-L. Wang and R. F. Sekerka, Phys. Rev. E **53**, 3760 (1996).
18. A. Karma and W.J.Rappel, Phys. Rev. Lett. **77**, 4050 (1996).
19. A. Karma and W.J.Rappel, Phys. Rev. E. **57**, 4323 (1998).
20. N. Provatas, N. Goldenfeld, J.A. Dantzig, Phys. Rev. Lett. **80**, 3308 (1998).
21. N. Provatas, N. Goldenfeld, J.A. Dantzig, J. Comput. Phys. **148**, 265 (1999).
22. V. L. Ginzburg and L. D. Landau, Soviet Phys. JETP **20**, 1064 (1950).
23. P. G. de Gennes, Mol. Cryst. Liq. Cryst. **12**, 193 (1971).
24. J. W. Cahn, J. E. Hilliard, J. Chem. Phys. **28**, 258 (1958).
25. J. W. Cahn, Acta Metall. **9**, 795 (1961).
26. J. W. Cahn and S. M. Allen, J. Phys. (Paris) Colloque **C7**, c7 (1977).
27. S. M. Allen and J. W. Cahn, Acta metall. mater. **27**, 1085 (1979).
28. R. J. Braun, J. W. Cahn, G. B. McFadden and A. A. Wheeler, Phil. Trans. Roy. Soc. London A **355**, 1787 (1997).
29. D. M. Anderson, G. B. McFadden, and A. A. Wheeler, Ann. Rev. Fluid Mech. **30**, 139 (1998).
30. J. S. Langer. Unpublished notes (1978).
31. J. S. Langer, in *Directions in Condensed Matter Physics*, ed. G. Grinstein, G. Mazenko (World Scientific, Philadelphia, 1986), pp. 165–186.
32. G. Caginalp, in *Applications of Field Theory to Statistical Mechanics*, ed. L Garrido, 216–226 Berlin: Springer-Verlag (1985).
33. J.B. Collins and H. Levine, Phys. Rev. B **31**, 6119 (1985).
34. G. Caginalp and P. C. Fife, Phys. Rev. B **33**, 7792 (1986).
35. G. Caginalp. Arch. Rat. Mech. Anal. **92**, 205 (1986).
36. G. Caginalp, Phys. Rev. A **39**, 5887 (1989).
37. O. Penrose and P.C. Fife, Physica D **43**, 44 (1990).
38. G. Caginalp and J. Jones, Appl. Math. Lett. **4**, 97 (1991).
39. G. Caginalp and J. Jones, in *On the Evolution of Phase Boundaries*, ed. M. E. Gurtin and G. B. McFadden, The IMA Series in Mathematics and Its Applications, Vol. 43 (Springer-Verlag, New York, 1992) pp. 27–50.
40. H. J. Diepers, C. Beckermann, and I. Steinbach, in *Solidification Processing*

1997, ed. J. Beech and H. Jones, Proc. 4th Decennial Int. Conf. on Solid. Process. (University of Sheffield, Sheffield, 1997) pp. 426–430.
41. C. Beckermann, H.-J. Diepers, I. Steinbach, A. Karma, and X. Tong, J. Comput. Physics **154**, 468 (1999).
42. R. Tönhardt, Convective Effects on Dendritic Solidification, 1998 Ph. D. thesis, Department of Mechanics, Royal Institute of Technology, S-100 44 Stockholm, Sweden.
43. R. Tönhardt and G. Amberg, J. Crystal Growth **194**, 406 (1998).
44. A. A. Wheeler and G. B. McFadden, Eur. J. Appl. Math. **7**, 367 (1996).
45. J. Lowengrub and J. Truskinovsky, Proc. Roy. Soc. Ser. A. **454**, 2617 (1998).
46. S.R. de Groot and P. Mazur, *Non-Equilibrium Thermodynamics* (Dover, New York, 1984).
47. A. P. Umantsev, J. Chem. Phys. **96**, 605 (1992).
48. S.-L. Wang, R.F. Sekerka, A.A. Wheeler, B.T. Murray, S.R. Coriell, R.J. Braun, and G.B. McFadden, Physica D **69**, 189 (1993).
49. D.W. Hoffman and J.W. Cahn, Surface Science **31**, 368 (1972).
50. J.W. Cahn and D.W. Hoffman, Acta Metallurgica **22**, 1205 (1974).
51. A.A. Wheeler and G.B. McFadden, Proc. Roy. Soc. Lond. A **453**, 1611 (1997).
52. G. B. McFadden, A. A. Wheeler and D. M. Anderson, Physica D. **144** 154 (2000).
53. C. Charach and P. C. Fife, Open Systems and Information Dynamics **5**, 99 (1998).
54. G. Caginalp, Phys. Rev. A 39, 5887 (1989).
55. A. Karma and W.-J. Rappel, Phys. Rev. E **53**, 3017 (1996).
56. D. M. Anderson, G. B. McFadden and A. A. Wheeler, A phase-field model with convection: sharp interface asymptotics; NISTIR 6568, National Institute of Standards and Technology, Gaithersburg, MD (October, 2000).
57. J.G. Blom, R.A. Trompert and J.G. Verwer, ACM Trans. Math. Software **22**, 302 (1996).
58. G.K. Batchelor, *An Introduction to Fluid Dynamics* (Cambridge University Press, Cambridge, 1970).
59. N.A. Ahmad, A.A. Wheeler, W.J. Boettinger, and G.B. McFadden, Physical Review E **58**, 3436 (1998).